JOURNAL OF SPACECRAFT AND ROCKETS
Vol. 38, No. 3, May–June 2001

Integrated Vibration Control for the Apparatus Cabin of CZ-3A Launch Vehicle

J. H. Zhang,* S. L. Xie,† and X. N. Zhang‡
Xi'an Jiaotong University, 710049 Xi'an, Shaanxi Province, People's Republic of China
and
Z. M. Li§
China Academy of Launch Vehicle Technology, 100076 Beijing, People's Republic of China

The vibration control of the apparatus cabin of CZ-3A launch vehicle is investigated. A kind of bar-type viscoelastic damper is designed to control passively the low-frequency vibrations of the whole cabin structure. Three strategies are employed to control the high-frequency vibrations of the honeycomb plate at different frequencies: passive control with the constrained damping layer, integrated control combining the constrained damping layer with the piezoelectric actuator designed by authors, and controllable constrained damping layer, respectively. The experimental results show that the present integrated techniques can effectively suppress the vibrations of the apparatus cabin within a fairly broad frequency band.

Nomenclature

C_{dR} = correction function
D = average diameter of viscoelastic damper
$\tilde{d}_e$ = effective piezoelectric coefficient
f = frequency
G = shear modulus
h = thickness of viscoelastic layer
k^* = complex stiffness
k_{dl} = dissipation stiffness
k_{dR} = storage stiffness
k'_{dR} = corrected storage stiffness
$\tilde{k}_e$ = effective dynamic stiffness
$\tilde{k}^*_e$ = effective electromechanical dynamic stiffness
l = length of viscoelastic damper
m = mass
$\boldsymbol{P}$ = external load in the axial direction
V = control voltage
$\boldsymbol{x}$ = displacement in the axial direction
$\tilde{Z}$ = effective impedance
α = ratio of length to average diameter
η = loss factor
ω = angular frequency

Introduction

THE apparatus cabin of CZ-3A launch vehicle is a large flexible space structure made up of bars, beams, a metallic platform, honeycomb plates, and honeycomb conic shell. It connects the rocket engine with the telemetric instruments and the gyroscope, which are installed on the honeycomb plates and the metallic platform, respectively. External excitations greatly influence the accuracy and reliability of these control devices because vibrational energy can be transferred from the apparatus cabin to them. Therefore, the vibrations of the apparatus cabin within the bandwidth (8–1000 Hz) of control instruments must be suppressed effectively for the safety of flight. Unfortunately, such large space structures are characterized by broad bandwidth, light damping, dense modes, and multimodes to be controlled.[1] In addition, light structure, low-energy consumption, and high economic efficiency must be considered in the control design of large space structures.

The past several decades have witnessed the developments of passive and active vibration control techniques. The passive technique is commonly used in structural vibration control due to advantages such as simple structure, high reliability, and low cost. However, it lacks flexibility to various control specifications. Active control can overcome the inherent shortcomings of passive control, but suffers from disadvantages such as low reliability, high cost, and the requirement of external power. Therefore, it seems that passive techniques and active techniques should not be considered independently in vibration control of large space structures. This has led to the development of integrated techniques in recent years,[2–5] which combine passive control with active control and may, consequently, improve performance, reliability, and control cost simultaneously.

This paper presents an investigation into the vibration control of the apparatus cabin of the CZ-3A launch vehicle. The integrated technique is employed. Model analyses of the whole cabin structure and the important components, including the honeycomb plates and the metallic platform are carried out experimentally, and lay the foundation of control design. The global modes and local modes are defined according to the structural deformations and motions, which may not be strict but provide guidance of the selection of the control manner. A kind of bar-type viscoelastic damper is designed to control the global modes passively. Three strategies are employed to perform integrated control of the local modes at different frequencies. Experimental results are discussed and conclusions are presented at the end of the paper.

Experimental Modal Analysis

Figure 1 shows a photograph of the apparatus cabin of CZ-3A launch vehicle. It consists of five types of components: 1) metallic bars and beams; 2) metallic platform A; 3) seven honeycomb plates B_i, $i = 1, \ldots, 7$; 4) honeycomb conic shell; and 5) viscoelastic damping pads. The maximum diameter of the cabin structure is about 3 m. The metallic platform and honeycomb plates lie on the top of the cabin and are supported by the metallic bars and beams.

The vibrations of the cabin structure subjected to external excitations can be transmitted to the control instruments that are installed on the metallic platform and honeycomb plates. To reveal the effects of vibrations of the apparatus cabin on these instruments and to perform control thereafter, modal analysis of the whole structure is carried out experimentally. The honeycomb plates and metallic platform are also individually tested in situ. The apparatus cabin is set on three evenly placed cushions, which simulates a free–free state. In the case of impulse excitations, the modal frequencies and

Received 18 November 1999; revision received 11 September 2000; accepted for publication 19 December 2000.

*Professor, Department of Engineering Mechanics; Zhangjh@xjtu.edu.cn.
†Lecturer, Theory of Lubrication and Bearing Institute; xieshilin@tlbi.xjtu.edu.cn.
‡Professor, Department of Engineering Mechanics; icapv@xjtu.edu.cn.
§Senior Engineer, First Institute.

Table 1 Elastic modes of the whole structure (5–500 Hz)

Mode	Frequency, Hz	Damping %
1	10.66	4.20
2	17.77	4.40
3	31.19	3.50
4	56.94	2.70
5	77.55	2.74
6	87.47	2.52
7	95.77	1.16
8	112.56	2.12
9	221.64	1.15
10	345.21	1.86
11	378.92	0.95
12	436.24	0.52
13	465.45	1.14

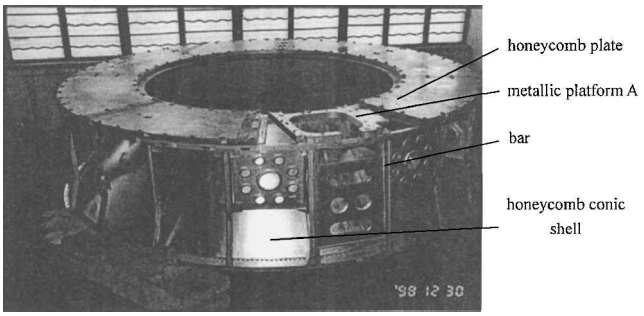

Fig. 1 Photograph of the apparatus cabin.

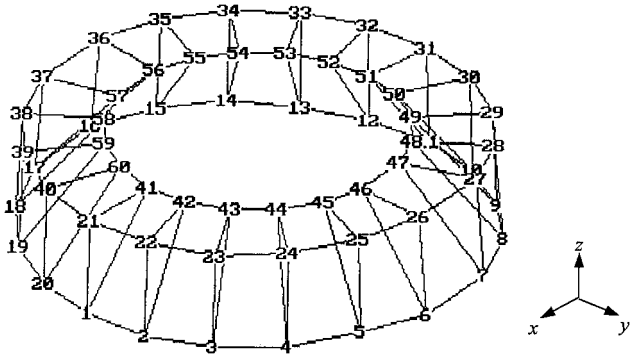

Fig. 2 Distribution of measurement points in the whole structure.

damping coefficients are computed by a Hewlett–Packard 3562 dynamic analyzer using the half-power point method.

Modal Analysis of the Whole Structure

The distribution of the measurement points in the modal analysis of the whole structure is shown in Fig. 2. The displacements of every point in both the radial and z directions are measured. The testing frequency ranges from 0.5 to 500 Hz.

The frequencies (in hertz) of the rigid-body motion are 1.4 in $x(y)$, 2.9 in the rotation around $x(y)$, 2.35 in the rotation around z, and 2.75 in z. The elastic modes of the whole structure are given in Table 1. The maximum rigid modal frequency (2.9 Hz) is only one-third of the first elastic modal frequency (10.66 Hz). Therefore, the coupling between the rigid vibrations and the elastic vibrations can be neglected.

For the elastic modes below 100 Hz, the components such as bars, beams, platform, honeycomb plates, and honeycomb conic shell all vibrate with large amplitudes. However, the elastic deformations of the honeycomb plates and platform are much smaller than those of other components. Therefore, the motions of the honeycomb plates and platform are assumed to be rigid, which means that they are mainly caused by the vibrations of other components. This is shown in Fig. 3, where the first elastic modal shape is given.

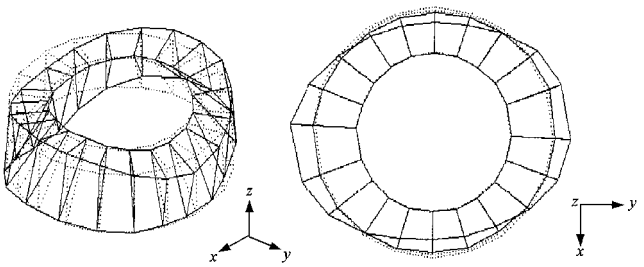

Fig. 3 First modal shape of the whole structure; f = 10.66 Hz.

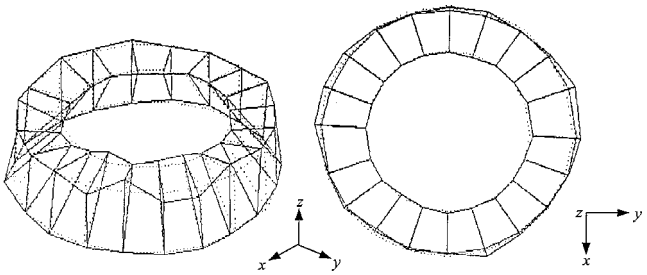

Fig. 4 Thirteenth modal shape of the whole structue; f = 465.45 Hz.

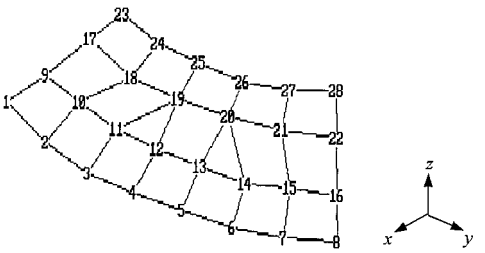

Fig. 5 Distribution of measurement points in honeycomb plate B_1.

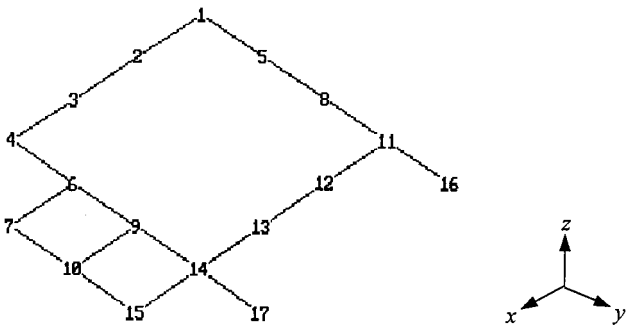

Fig. 6 Distribution of measurement points in platform A.

For the elastic modes above 100 Hz, the vibrations of the honeycomb plates and metallic platform are dominant due to the larger elastic deformations. In addition, the higher the frequency, the more apparent this dominance becomes, as seen in Fig. 4, where the 13th elastic modal shape is shown. This recommends individual modal analysis of the honeycomb plates and the platform in the high-frequency domain.

Modal Analysis of the Components

One of the honeycomb plates, B_1, and metallic platform A are tested in situ, respectively. The corresponding distributions of measurement points are shown in Figs. 5 and 6, respectively. Only the displacement in the z direction of every point is measured. The testing frequencies range from 100 to 700 Hz for honeycomb plate B_1 and from 100 to 1000 Hz for platform A.

The results of the modal analyses are given in Tables 2 and 3. The modal shape of honeycomb plate B_1 at 235.02 Hz, and that of platform A at 106.31 Hz are shown in Figs. 7 and 8, respectively, from which it is seen that the two components deform significantly.

Table 2 Modes of honeycomb plate B_1 (100–700 Hz)

Frequency, Hz	Damping %
105.14	0.93
108.38	0.79
113.69	1.11
135.01	0.86
152.73	0.34
176.29	0.28
201.83	2.32
224.95	1.35
235.02	1.16
252.99	1.78
268.15	1.71
273.98	0.41
308.84	1.90
344.03	2.12
361.23	1.75
374.69	1.12
402.45	1.65
433.16	0.68
448.53	1.98
463.11	1.17
487.30	1.14
550.82	2.31
629.01	1.67
682.40	1.46

Table 3 Modes of metallic platform A (100–1000 Hz)

Frequency, Hz	Damping, %
103.24	0.62
106.31	0.80
108.26	0.91
134.73	0.87
149.12	0.41
164.42	0.88
174.73	0.66
178.80	0.18
186.60	0.57
210.04	1.12
225.21	1.54
235.30	0.76
259.00	0.54
277.87	0.84
294.54	0.45
304.04	0.92
348.70	1.59
380.11	0.54
437.26	1.16
468.22	1.92
538.34	1.19
592.66	1.07
649.63	1.57
671.96	0.75
698.77	0.66
892.56	0.45
929.31	1.86

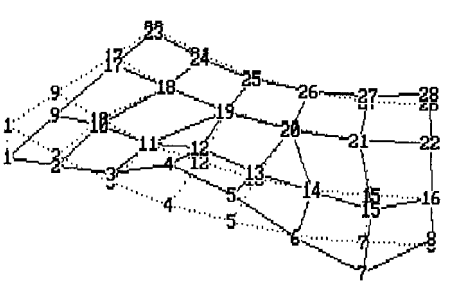

Fig. 7 Modal shape of honeycomb plate B_1; f = 235.02 Hz.

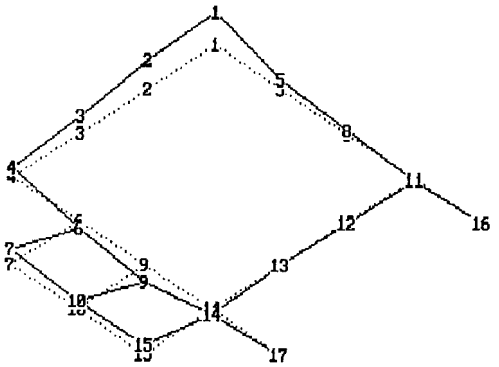

Fig. 8 Modal shape of platform A; f = 106.31 Hz.

Global Modes and Local Modes

From the results of modal analyses shown earlier, it is seen that the vibrations of honeycomb plate B_1 and metallic platform A are caused by two factors, the motions and deformations of other components and the elastic deformations themselves. For honeycomb plate B_1 and metallic platform A, the vibrations at frequencies less than 100 Hz result mainly from the former factor, and those at frequencies greater than 100 Hz mainly from the latter. Therefore, the cabin structure influences the operations of the control instruments primarily in two forms, namely, global vibrations in the low-frequency domain and local vibrations in the high-frequency domain.

For clarity, we define the low-frequency modes (<100 Hz) of the whole structure as the global modes and the high-frequency modes (>100 Hz) of honeycomb plate B_1 and metallic platform A as the local modes. These definitions are not strict but do provide guidance for the selection of control manner as seen in the following sections. To suppress effectively the vibrations of the apparatus cabin structure, it is obvious that the global modes and local modes all should be considered as control objects.

Control of the Global Modes

The vibrations of components such as bars and beams should be suppressed greatly because of their dominance in the global modes. Research in recent years has shown that passive control with bar-type viscoelastic dampers is a promising method for structures that are made up of bars or beams.[6] In this section, a kind of bar-type viscoelastic damper is designed to control the global modes passively by attenuating the vibrations of the bars and beams.

Design of Bar-Type Viscoelastic Damper

Figure 9 shows the configuration and dynamic model of the bar-type viscoelastic damper, where k^* is expressed as

$$k^* = k_{dR} + jk_{dl} \tag{1}$$

The loss factor η is defined as

$$\eta = k_{dl}/k_{dR} \tag{2}$$

The equation of motion can be written as

$$m\ddot{\boldsymbol{x}} + k_{dR}(1 + j\eta)\boldsymbol{x} = \boldsymbol{P} \tag{3}$$

It is shown from Eq. (3) that storage stiffness k_{dR} and loss factor η can characterize the viscoelastic damper. They depend on factors such as viscoelastic material property, configuration and dimension of the damper, vibrational frequency, and environmental temperature. The following assumptions are made to approximate the storage stiffness: 1) The centric bar and crust of the viscoelastic damper are rigid bodies. 2) The external excitations are in the axial direction. 3) The shear deformations in the radial direction are linear with the radial positions. 4) The environmental temperature is 25°C. Therefore, we have

$$k_{dR} = \pi\alpha D^2 G/h \tag{4}$$

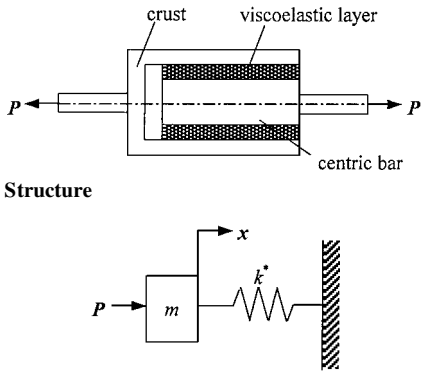

Fig. 9 Configuration of viscoelastic damper.

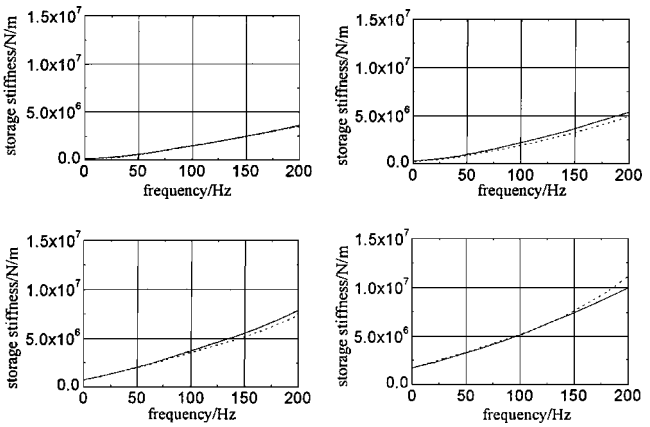

Fig. 10 Predicted and experimental values of storage stiffness: ——, experimental value, and - - -, predicted value.

where G is the shear modulus depending on the vibrational frequency. In practice, storage stiffness k_{dR}, computed from Eq. (4), may deviate from the measured value. Here a correction factor, $C_{dR}(f)$, is introduced to Eq. (4), that is,

$$k'_{dR} = C_{dR}(f)\pi\alpha D^2 G/h \tag{5}$$

where $C_{dR}(f)$ is a quadratic polynomial of frequency f and can be obtained by fitting the experimental data. Figure 10 shows the predicted values from Eqs. (4) and (5) and the experimental values of the storage stiffness for four bar-type viscoelastic dampers with different dimensions. It is obvious that the corrected values agree well with experimental ones. Therefore, the actual dimension of the bar-type viscoelastic damper can be determined from Eq. (5) when the storage stiffness is given.

Passive Control with Viscoelastic Dampers

Two bar-type viscoelastic dampers are designed based on Eq. (5) and thereafter placed at the rim of the cabin structure. In Fig. 2, one damper serves as the link between measurement points 33 and 15 and the other damper as the link between measurement points 32 and 10, where the vibrations of the bars and beams are remarkable for most of the global modes.

Figure 11 shows the frequency responses of measurement point 33 from 5 to 105 Hz for the controlled and uncontrolled cases when a sinusoidal swept excitation is applied on measurement point 6 in the z direction. It is seen from Fig. 11 that the global modes at 10.66, 31.19, 56.94, and 95.77 Hz are all suppressed effectively. Especially, the amplitude of the mode at 31.19 Hz is reduced by 68.87%. This indicates the effectiveness of passive control with the bar-type viscoelastic dampers for the global modes.

Control of the Local Modes

The local modes involve significant local deformations of honeycomb plate B_1 and platform A and are, therefore, controllable from the locations of these components. This section investigates the control of the local modes for honeycomb plate B_1, in which three strategies are presented for different frequencies and the integration of passive and active techniques is emphasized.

Table 4 Local modes for the uncontrolled and controlled cases (100–200 Hz)

Frequency, Hz (uncontrolled)	Damping,% (uncontrolled)	Frequency, Hz (controlled)	Damping,% (controlled)
105.14	0.93	105.64	1.33
108.38	0.79	109.27	1.05
113.69	1.11	115.05	1.59
135.01	0.86	136.58	1.47
152.73	0.34	154.42	0.68
176.29	0.28	178.38	1.08

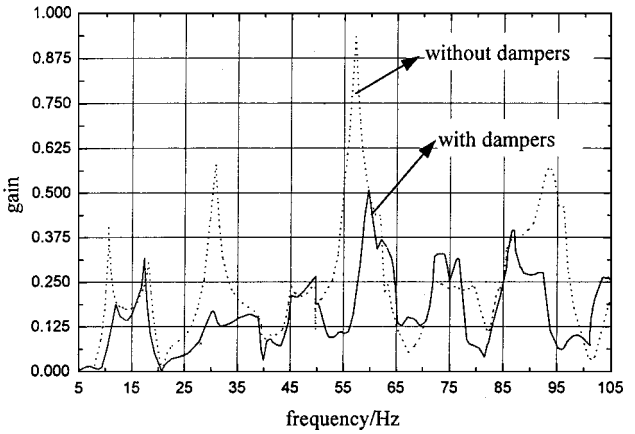

Fig. 11 Experimental frequency response under passive control with dampers.

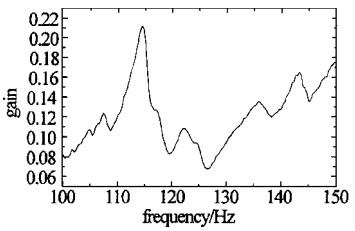

Fig. 12 Experimental frequency response under passive control with constrained damping layer.

Passive Control with Constrained Damping Layer

A constrained damping layer is used to control passively the local modes of honeycomb plate B_1. Seven honeycomb plates are all covered with the constrained damping layer. The damping layer is made from ZN-1 viscoelastic material and is 0.001 m in thickness, whereas the constraining layer is made from stainless steel and is 0.0005 m in thickness. The frequencies and damping coefficients of the local modes for honeycomb plate B_1 in the controlled and uncontrolled cases are given in Table 4. It is seen from Table 4 that the damping coefficients of the local modes ranging from 100 to 200 Hz all increase to some extent under passive control. In addition, the higher the frequency, the more significantly the damping coefficient increases, which means that the constrained damping layer is more effective for the local modes at higher frequencies.

A sinusoid swept excitation is applied in the z direction at measurement point 12 (Fig. 5). The corresponding acceleration frequency response in the same direction at measurement point 13 is given in Fig. 12. It is shown that the amplitude of the 115.05-Hz mode, which is in the lower frequency domain, is much larger than those of the rest of the local modes. To suppress the 115.05-Hz local mode further, active control is introduced in the following sections.

Integrated Control with Piezoelectric Actuator

The local modal vibrations in the lower frequency domain are partly caused by the motions of the bars and beams in spite of the

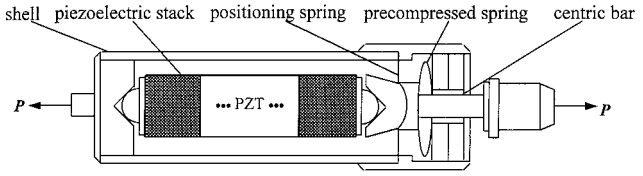

Fig. 13 Configuration of the piezoelectric actuator.

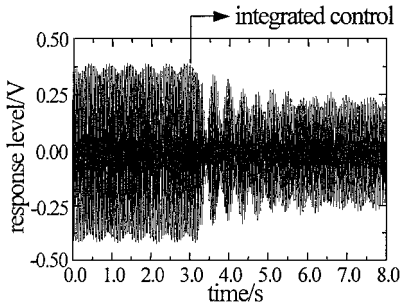

Fig. 14 Time response under integrated control with piezoelectric stack actuator.

dominance of elastic deformation of honeycomb plate B_1. Therefore, the control of the motions of the bars and beams may result in further attenuation of the 115.05-Hz local mode. The piezoelectric stack actuator is commonly used to control actively the structures that are made up of bars or beams because of the advantages of small displacement and great output force.[7,8] In this subsection, a piezoelectric stack actuator is designed and thereafter combined with the constrained damping layer to perform integrated control for the 115.05-Hz local mode.

Design of Piezoelectric Actuator

Figure 13 shows the configuration of piezoelectric stack actuator, which consists of piezoelectric stack, positioning spring, precompressed spring, centric bar, and shell. Its electromechanical dynamic characteristic can be described by

$$\boldsymbol{x} = \boldsymbol{P}\big/\tilde{k}_e^* + \tilde{d}_e V \tag{6}$$

where V is the control voltage applied on the piezoelectric stack and the effective electromechanical dynamic stiffness $\tilde{k}_e^{\bullet}$ can be written as

$$\tilde{k}_e^* = \tilde{k}_e \big/ \left(1 - j\omega \tilde{k}_e \tilde{d}_e^2 \tilde{Z}\right) \tag{7}$$

where $\tilde{k}_e$ is the effective dynamic stiffness of the actuator depending on the effective dynamic stiffness of the piezoelectric stack and the stiffness of elastic components in series with it and $\tilde{Z}$ is the effective impedance determined by the resistance in parallel with the actuator and the effective dynamic capacitance of the actuator. The capability of the piezoelectric stack actuator can be characterized by the dynamic displacement gain and dynamic force gain, which are obtained from Eq. (6) when the boundary conditions of the actuator are free–free and fixed–free, respectively.

Control Experiment

The major performance indices of the piezoelectric stack actuator are as follows: the maximum working voltage is 40 V, the maximum displacement gain and the maximum force gain are 103.89 nm/V and 1.64 N/V, respectively, and the working frequency ranges from 5 to 1000 Hz. It serves as the link between measurement points 3 and 24 (Fig. 2), where honeycomb plate B_1 is located. A proportional feedback strategy is employed in the active control, which is implemented on a digital processor (CPU 166 MHz).

Figure 14 shows the time history of the displacement of measurement point 13 (Fig. 5) in the z direction when the 115.05-Hz sinusoid excitation in the same direction is applied on measurement point 12 (Fig. 5). The control voltage applied on the piezoelectric actuator is 10 V. Figure 14 shows that the vibrational amplitude of measurement point 13 at 115.05 Hz is reduced by 20% under integrated control. However, the control performance improves a little with the increase in control voltage, which indicates the limited capability of the integrated control with the piezoelectric actuator to suppress the local modal vibrations in the lower frequency domain.

Integrated Control with Controllable Constrained Damping Layer

The controllable constrained damping layer is a new integration method developed in recent years.[9,10] Figure 15 shows the configuration of the controllable constrained damping layer, which is made up of piezoelectric patches, constrained layer, viscoelastic damping layer, and the structure under control. The controlled structure is covered with the viscoelastic damping layer and the constrained layer. The piezoelectric patches made from Pmn piezocrystal ceramics are adhered to the constrained layer and act as actuators that increase the shear deformation of the viscoelastic layer by deforming the constrained layer and thereby can damp the structure under control. In comparison with active constrained layer damping,[11–13] the controllable constrained damping layer demands piezoelectric actuators of smaller area and lower cost. Therefore, it provides a preferable integration method for vibration control of the structures that have been covered with the constrained damping layer.

In this subsection, the controllable constrained damping layer is used to control the 115.05-Hz local mode. The 115.05-Hz mode involves significant local bending of honeycomb plate B_1 as seen from Fig. 16, where the corresponding modal shape is given. Therefore, 10 piezoelectric patches are placed in the middle of honeycomb plate B_1, as shown in Fig. 16, where the large surface strain occurs. Each piezoelectric patch is 0.02 m in width, 0.03 m in length and 0.00075 m in thickness. A B&K4370 accelerometer is placed between measurement points 12 and 13 and acts as the sensing device. A proportional feedback scheme is used in the active control.

Figure 17 shows the time history of displacement of measurement point 13 (Fig. 5) in the z direction when the 115.05-Hz sinusoid

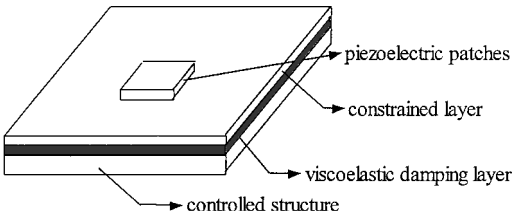

Fig. 15 Configuration of the controllable constrained damping layer.

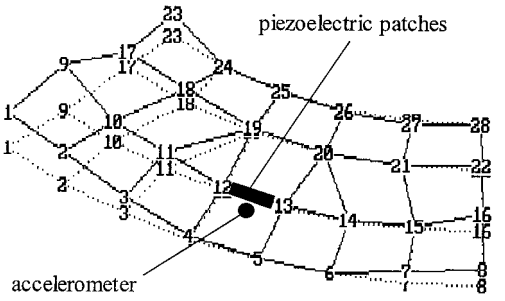

Fig. 16 Modal shape of honeycomb plate B_1; f = 115.05 Hz.

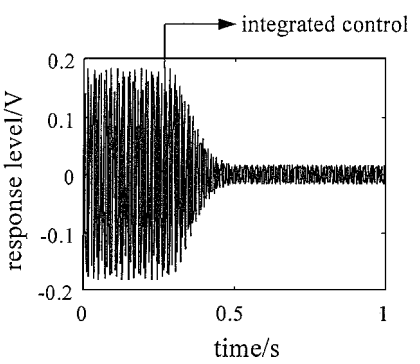

Fig. 17 Time response under integrated control with controllable constrained damping layer.

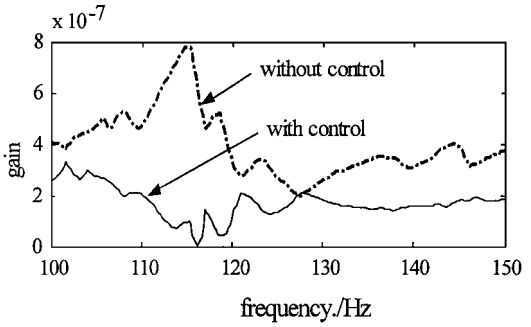

Fig. 18 Experimental frequency responses under the passive and integrated control.

excitation in the same direction is applied on measurement point 12 (Fig. 5). It can be seen that the vibrational amplitude of measurement point 13 at 115.05 Hz is reduced by 90% under the integrated control with the control voltage of 89 V. In addition, the acceleration frequency response from 100 to 150 Hz of measurement point 13 in the same experimental condition is given in Fig. 18. It is shown that the local modes from 100 to 150 Hz are all suppressed effectively; in particular, the amplitude of the 115.05-Hz mode is reduced by 80%.

Conclusions

The vibrations of the apparatus cabin of CZ-3A launch vehicle in the wider frequency band have been suppressed effectively. It is accomplished in two ways, namely, passive control of the global modes and integrated control of the local modes.

The dominance of global vibrations for the global modes recommends that the motions and elastic deformations of the bars and beams should be attenuated greatly. The experimental results validate the efficiency of passive control with bar-type viscoelastic dampers for the global modes.

The passive control with constrained damping layer can significantly suppress the high-frequency local modes but has less effect on the low-frequency local modes, which suggests the employment of the integrated technique. The integrated control, combining the constrained damping layer with the piezoelectric actuator, exhibits limited capability, probably due to smaller deformations of the bars and beams involved in the low-frequency local modes. In contrast, the controllable constrained damping layer can suppress the low-frequency local modes effectively.

Acknowledgments

The research is supported by National Natural Science Foundation of China (Grant 19632001). We appreciate greatly the China Academy of Launch Vehicle Technology for providing the test specimens. We are also very grateful to G. Lu, J. B. Li, and F. Lu for their efficient cooperation.

References

[1]Balas, M. J., "Trends in Large Space Structure Control Theory: Fondest Hopes, Wildest Dreams," *IEEE Transactions on Automatic Control*, Vol. 27, No. 3, 1982, pp. 522–535.

[2]Gaudreault, M. L. D., Liebst, B. S., and Bagley, R. L., "Simultaneous Design of Active Vibration Control and Passive Viscous Damping," *Journal of Guidance, Control, and Dynamics*, Vol. 17, No. 4, 1994, pp. 879, 880.

[3]Mohamed, A. R., and Khaleefi, A. L., "Feasibility of Active and Passive Pulse Control for Flexible Structures," *Journal of Vibration and Control*, Vol. 1, No. 3, 1995, pp. 273–289.

[4]Garcia, E., Webb, S., and Duke, J., "Passive and Active Control of a Complex Flexible Structure Using Reaction Mass Actuators," *Journal of Vibration and Acoustics*, Vol. 117, No. 2, 1995, pp. 116–122.

[5]Huang, W. H., Wang, X. Q., Zhang, J. H., and Zheng, G. T., "Several Advances in Vibration Control of Aerospace Structures," *Advances in Mechanics*, Vol. 27, No. 1, 1997, pp. 5–18 (in Chinese).

[6]Lu, G., Li, J. B., Lu, F., and Zhang, J. H., "An Experimental Study on the Dynamic Design and Application of Viscoelastic Dampers," *Journal of Experimental Mechanics*, Vol. 13, No. 2, 1998, pp. 190–196, (in Chinese).

[7]Rao, S. S., and Sunar, M., "Piezoelectricity and Its Use in Disturbance Sensing and Control of Flexible Structures: A Survey," *Applied Mechanics, Reviews*, Vol. 47, No. 4, 1994, pp. 113–123.

[8]Main, J. A., and Garcia, E., "Piezoelectric Stack Actuators and Control System Design: Strategies and Pitfalls," *Journal of Guidance, Control, and Dynamics*, Vol. 20, No. 3, 1997, pp. 479–485.

[9]Zhang, X. N., Chen, L., Li, Z. M., and Zhang, J. H., "Vibration Hybrid Control of Plate with Controllable Constrained Damping Layer," *Journal of Applied Mechanics*, Vol. 16, No. 3, 1999, pp. 86–92 (in Chinese).

[10]Zhang, X. N., "Controllable Constrained Damping Layer and Its Application in Aerospace Structures," Ph.D Dissertation, Xi'an Jiaotong Univ., Xiýan, PRC, Jan. 1999.

[11]Baz, A., "Optimization of Energy Dissipation Characteristic of Active Constrained Layer Damping," *Smart Materials and Structures*, Vol. 6, No. 3, 1997, pp. 360–368.

[12]Shen, I. Y., "A Variational Formulation, a Work-Energy Relation and Damping Mechanisms of Active Constrained Layer Treatments," *Journal of Vibration and Acoustics*, Vol. 119, No. 2, 1997, pp. 192–199.

[13]Liao, W. H., and Wang, K. W., "A New Active Constrained Layer Configuration with Enhanced Boundary Actions," *Smart Materials and Structures*, Vol. 5, No. 5, 1996, pp. 638–648.

R. B. Malla
Associate Editor